Optimum PR Control Applied to *LCL* Filters With Low Resonance Frequency

Roberto A. Fantino, Claudio A. Busada, and Jorge A. Solsona, *Senior Member, IEEE*

***Abstract*—A control strategy for *LCL* grid-connected voltage source inverters is proposed. Using the injected grid current measurement exclusively, the proposal allows the use of the proportional plus resonant regulator optimum design, regardless of the filter resonance frequency. Simulation and experimental results that demonstrate the validity and effectiveness of the proposal for different *LCL* filter resonance frequency values are presented. Also its superiority compared with a control method recently proposed in the literature is shown.**

***Index Terms*—Active damping, *LCL* filter, low resonance frequency, proportional plus resonant (PR) control, voltage-source inverter.**

I. Introduction

VOLTAGE-SOURCE inverters (VSI) are widely used in distributed generation systems for grid current injection. In order to meet the power quality requirements [1]–[3], the inverter must be linked to the grid via a suitable filter. It is common to use a simple inductor (*L* filter). Nevertheless, to meet the power quality requirements with this kind of filter requires a high inductance value or a high switching frequency. For this reason, it is preferable to use *LCL* filters (see Fig. 1), which offer advantages in terms of cost and size reduction. However, the natural resonance frequency $\omega_{\rm res}^L$ of the *LCL* filters difficults the current grid injection control. The lower the filter resonance frequency, the greater the attenuation of the inverter switching frequency. Nonetheless, the difficulty in controlling the filter will increase. Many methods have been proposed and studied to damp this resonance. These methods can be classified into passive damping [4], [5] and active damping [6]–[16]. Passive damping introduces power losses to the system (reducing efficiency). For this reason, when the filter resonance frequency is located within the control bandwidth, it is generally preferred to use active damping.

Many different control techniques for *LCL* filters have been proposed in the literature such as: multiloop control strategies [17], full-state feedback control [18], [19], adaptive control [20], or neural networks control [21]. Some of these techniques are very complex and some of them require the use of additional sensors to those needed to control an *L* filter. Given the need to reduce the complexity of the controller and the number of sensors, [9] shows that it is possible to control a high resonance frequency *LCL* filter feeding back only grid current measurement $\vec{i}_{2_{abc}}$ (see Fig. 1).

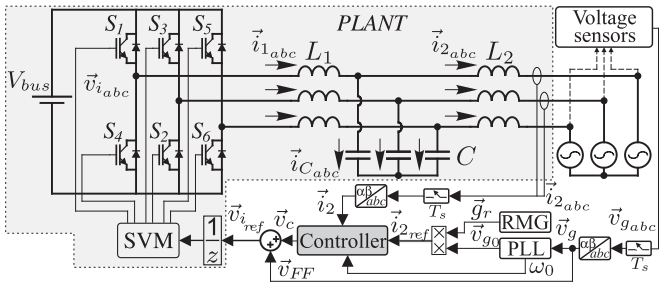

Fig. 1. Three-phase VSI linked to the grid via an *LCL* filter.

Following this line, in [10] the *LCL* filter control using a proportional plus resonant (PR) [22]–[25] was analyzed. It was proved in [10] that there exists a critical resonance frequency $\omega_{\rm crit}$, such that:

1) if $\omega_{\rm res}^L > \omega_{\rm crit}$, it is possible to control the system with a PR regulator with $\vec{i}_{2_{abc}}$ feedback only;
2) if $\omega_{\rm res}^L < \omega_{\rm crit}$ feedback of capacitor current measurement $\vec{i}_{C_{abc}}$ is additionally required [11], [15];
3) if $\omega_{\rm res}^L = \omega_{\rm crit}$, the system will be unstable even if $\vec{i}_{C_{abc}}$ feedback is implemented.

It is interesting to be able to control an *LCL* filter with $\omega_{\rm res}^L \leq \omega_{\rm crit}$, employing $\vec{i}_{2_{abc}}$ feedback only. In [14], this is achieved using a PR controller plus an active damping loop that feeds $\vec{i}_{2_{abc}}$ back through a first-order high-pass filter (HPF) [12]–[14]. However, when this method is used to control an *LCL* filter with very low resonance frequency, it will be shown in this paper that a poor dynamic response of the closed-loop system is obtained.

This paper proposes a current control strategy that allows to control an *LCL* filter with $\vec{i}_{2_{abc}}$ feedback only, regardless of the *LCL* filter resonance frequency value. The controller is based on the following idea: applying reference model control techniques [26] to an *LCL* filter with a low resonance frequency $\omega_{\rm res}^L < \omega_{\rm crit}$, a system that emulates the behavior of an *LCL* filter with a high resonance frequency $\omega_{\rm res}^L > \omega_{\rm crit}$ can be obtained. In concordance with [10] the system obtained can be controlled using a PR regulator. Furthermore, it will be shown that if the resonance frequency of the emulated filter

Manuscript received October 3, 2016; revised December 13, 2016; accepted February 2, 2017. Date of publication February 9, 2017; date of current version October 6, 2017. This work was supported in part by the Universidad Nacional del Sur, in part by Consejo Nacional de Invertigaciones Científicas y Técnicas (CONICET) and in part by Agencia Nacional de Promoción Científica y Tecnológica (ANPCyT), Argentina. Recommended for publication by Associate Editor F. Gao.

The authors are with Instituto de Investigaciones en Ingeniería Eléctrica and Departamento Ingeniería Eléctrica y de Computadoras, Universidad Nacional del Sur CONICET, Bahía Blanca 8000, Argentina (e-mail: rafantino@gmail.com; cbusada@uns.edu.ar; jsolsona@uns.edu.ar).

Digital Object Identifier 10.1109/TPEL.2017.2667409

is properly selected, the control can be implemented using an optimum design of the PR regulator [23]. Both simulation and experimental results of the proposed controller are presented, and its performance is evaluated against the controller design presented in [14]. From this comparison it is concluded that the proposal presented here offers better closed-loop dynamic response and better disturbance rejection.

II. System Description and Modeling

Fig. 1 shows the circuit diagram of a three-phase grid-connected VSI, powered by a constant dc voltage source $V_{\rm bus}$. The output voltage of the inverter is connected to the grid via a three-phase *LCL* filter, composed of inductors L_1, capacitors C, and inductors L_2. Sensors are used to measure the three-phase grid voltage $\vec{v}_{g_{abc}}$, and the three-phase current injected to the grid $\vec{i}_{2_{abc}}$. Measurements are transformed into the $\alpha\beta$ reference frame. In this frame, the current vector injected to the grid will be called $\vec{i}_2$, the grid voltage vector will be called $\vec{v}_g$, and the inverter side voltage vector applied to the filter will be called $\vec{v}_i$.

The aim of the "Controller" block shown in Fig. 1 is to regulate $\vec{i}_2$, for controlling the power flow from the dc voltage source $V_{\rm bus}$ to the grid. The current reference $\vec{i}_{2_{\rm ref}}$ is synchronized with the positive-sequence fundamental component $\vec{v}_{g_0}$ of $\vec{v}_g$. This reference is generated multiplying a vector gain $\vec{g}_r$, obtained from the reference magnitude generator (RMG) block, by the component $\vec{v}_{g_0}$ detected using a phase-locked loop (PLL) block. In addition, the PLL block identifies the fundamental angular grid frequency ω_0, which is used to tune the resonance frequency of the PR regulator. The behavior of current $\vec{i}_2$, can be modeled by the following continuous system:

$$\vec{i}_2(s) = G^L_{\rm dir}(s)\vec{v}_i(s) + \vec{i}_{2_{\rm per}}(s) \tag{1}$$

where $\vec{i}_{2_{\rm per}}$ is the component of $\vec{i}_2$ produced by disturbance $\vec{v}_g$, and $G^L_{\rm dir}(s)$ is the transfer function

$$G^L_{\rm dir}(s) = \left.\frac{\vec{i}_2(s)}{\vec{v}_i(s)}\right|_{\vec{i}_{2_{\rm per}}(s)=0} = \frac{{\omega^L_{\rm res}}^2}{sL_T(s^2+{\omega^L_{\rm res}}^2)} \tag{2}$$

where $L_T = (L_1 + L_2)$ and $\omega^L_{\rm res} = \sqrt{L_T/(L_1L_2C)}$ is the *LCL* filter resonance frequency. In order to model the discrete-time system behavior with sampling period T_s, a one sample delay z^{-1} cascaded with the controller (block $1/z$ in Fig. 1) is considered, which takes into account the digital processing delay [23], [27], [28]. Using the zero-order-hold method [10], [29] to obtain the *Z*-transform of (2), the discrete time transfer function of the plant $G^L(z) = z^{-1}G^L_{\rm dir}(z)$ is found

$$G^L(z) = \frac{\vec{i}_2(z)}{\vec{v}_{i_{\rm ref}}(z)} = \frac{T_s}{L_T}\frac{\left[z^2 - 2z\cos(\omega^L_{\rm res}T_s)+1\right] - b(z-1)^2}{z(z-1)\left[z^2-2z\cos(\omega^L_{\rm res}T_s)+1\right]} \tag{3}$$

where $b = \sin(\omega^L_{\rm res}T_s)/(\omega^L_{\rm res}T_s)$. Considering a stiff grid condition [30], a feedforward compensation $\vec{v}_{\rm FF} = \vec{v}_g$ can be used to counteract the effect produced by disturbance $\vec{v}_g$ on current $\vec{i}_2$ [23] (see Fig. 1). In such a case, the voltage reference applied to the inverter result $\vec{v}_{i_{\rm ref}}(z) = \vec{v}_c(z) + \vec{v}_{\rm FF}(z)$. The behavior of $\vec{i}_2(z)$ can be modeled as a function of the control action $\vec{v}_c(z)$ as

$$\vec{i}_2(z) = G^L(z)\vec{v}_c(z) + \vec{i}_{2_{\rm per}}(z) \tag{4}$$

with $\vec{i}_{2_{\rm per}}(z) = G^L(z)\vec{v}_{\rm FF}(z) + \vec{i}_{2_{\rm per}}(z)$. In order to simplify the analysis of the control loop behavior, in what follows it is assumed that $\vec{i}_{2_{\rm per}} = 0$ (no external disturbance).

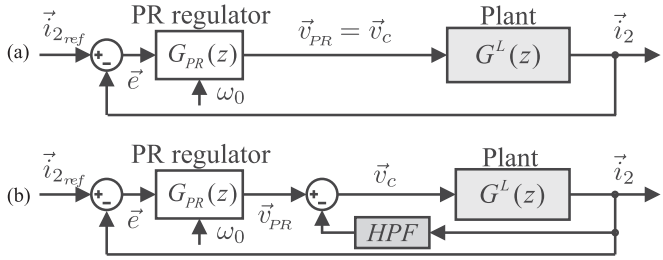

Fig. 2. Control of the system of Fig. 1. (a) Using only a PR regulator (for $\omega^L_{\rm res} > \omega_{\rm crit}$). (b) Using a PR plus a first-order HPF.

III. Control Using a PR Regulator

According to the internal model principle [31], to copy a reference $\vec{i}_{2_{\rm ref}}$ without steady-state error at the fundamental angular grid frequency ω_0, it is common to use a PR regulator with its resonance tuned at that frequency [22]. Fig. 2(a) shows the block diagram of the system of Fig. 1, when the "Controller" block is implemented using a PR regulator. The PR discrete transfer function, obtained with the Tustin transform method with prewarping [10], [29], is given by

$$G_{PR}(z) = \frac{\vec{v}_{PR}(z)}{\vec{e}(z)} = K_p\left(1 + \frac{a}{T_r}\frac{z^2-1}{z^2 - 2z\cos(2\pi\omega_0/\omega_s)+1}\right) \tag{5}$$

where $a = \sin(\omega_0 T_s)/(2\,\omega_0)$ and $\omega_s = 2\pi/T_s$ is the sampling angular frequency; $\vec{v}_{\rm PR}(z)$ and $\vec{e}(z)$ are defined in Fig. 2.

In [23], an optimum design for a PR regulator used to control an L filter (considering the digital processing delay) was proposed. If L_T is the inductance value of the L filter, to obtain a system with a desired phase margin $\phi_m \approx 45^\circ$ at a resulting crossover frequency $\omega_c \approx \omega_s/12$, the PR parameters must be [10], [23]

$$K_{p_{\rm opt}} = \frac{\omega_s L_T}{12} \quad \& \quad T_{r_{\rm opt}} = \frac{120}{\omega_s} \tag{6}$$

In [10], two significant regions for the control of an *LCL* filter using a PR were identified. These regions are delimited by the critical resonance frequency $\omega_{\rm crit} = \omega_s/6 \approx 0.17\,\omega_s$. If $\omega^L_{\rm res} > \omega_{\rm crit}$ (high resonance frequency region), the system of Fig. 2(a) is stable. On the other hand, if $\omega^L_{\rm res} < \omega_{\rm crit}$ (low resonance frequency region), the system is unstable. To achieve system stability in the latter region, it is shown in [10] that the additional feedback (and the consequent measurement) of capacitor current $\vec{i}_{C_{abc}}$ (see Fig. 1) is required. Another alternative to stabilize the control loop is the feedback of current $\vec{i}_2$ toward the system

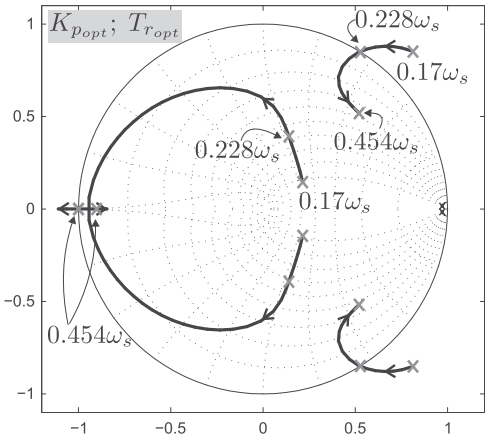

Fig. 3. Root locus of the closed-loop system of Fig. 2(a) with $K_p = K_{p_{\rm opt}}$ and $T_r = T_{r_{\rm opt}}$, as a function of $\omega^L_{\rm res}$.

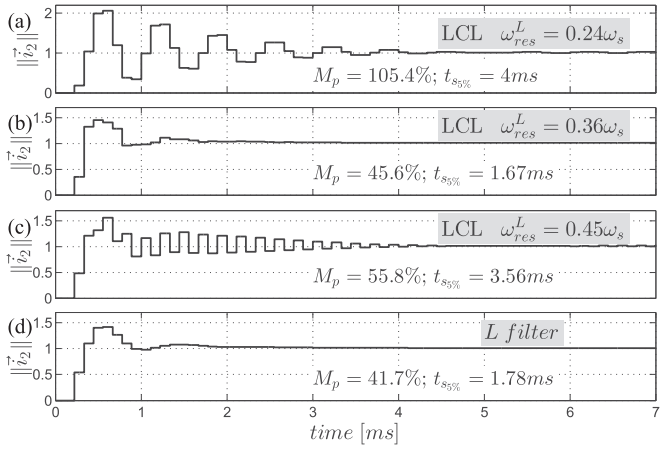

Fig. 4. Step response of the system of Fig. 2(a) with $K_p = K_{p_{\rm opt}}$ and $T_r = T_{r_{\rm opt}}$ for filters: (a) *LCL* with $\omega^L_{\rm res} = 0.24\,\omega_s$, (b) *LCL* with $\omega^L_{\rm res} = 0.36\,\omega_s$, (c) *LCL* with $\omega^L_{\rm res} = 0.45\,\omega_s$, and (d) *L* Vertical Axes [A].

input, through a first-order HPF [12]–[14], as it is shown in Fig. 2(b).

The high resonance frequency region $\omega^L_{\rm res} > \omega_{\rm crit}$ is the zone where the closed-loop system of Fig. 2(a) is stable. However, it should be noted that for $K_p = K_{p_{\rm opt}}$, the range of $\omega^L_{\rm res}$ where such system is stable, is smaller. In order to know the range of $\omega^L_{\rm res} > \omega_{\rm crit}$ where the system is stable by using the PR optimum design (6), Fig. 3 has been drawn. This figure shows the root locus of the closed-loop system as a function of $\omega^L_{\rm res}$, when a PR with $K_p = K_{p_{\rm opt}}$ and $T_r = T_{r_{\rm opt}}$ is used. It shows that the stability range is $0.228\,\omega_s \le \omega^L_{\rm res} \le 0.454\,\omega_s$. To verify the stability within this range, Fig. 4(a)–(c) shows the unit step responses of the system of Fig. 2(a) with $K_p = K_{p_{\rm opt}}$ and $T_r = T_{r_{\rm opt}}$ for *LCL* filters with resonance frequency: (a) $\omega^L_{\rm res} = 0.24\,\omega_s$; (b) $\omega^L_{\rm res} = 0.36\,\omega_s$; and (c) $\omega^L_{\rm res} = 0.45\,\omega_s$. These responses were obtained, applying to the system of Fig. 2(a) a positive-sequence unit magnitude current reference vector $\vec{i}_{2_{\rm ref}}$, with angular frequency ω_0, at the instant $t > 0$. In each case it is indicated that the percentage overshoot relative to the final value (M_p) and the settling time with a threshold value of 5% ($t_{s_{5\%}}$). For comparison, Fig. 4(d) shows the unit step response obtained when an *L* filter is controlled with the PR optimum design [23]. Note that for the intermediate angular frequency $\omega^L_{\rm res} = 0.36\,\omega_s$ [see Fig. 4(b)] the values of M_p and $t_{s_{5\%}}$ are very similar to those obtained with the *L* filter [see Fig. 4(d)]. Note also that for $\omega^L_{\rm res} \neq 0.36\,\omega_s$ [see Fig. 4(a) and (c)] the response is degraded.

IV. Proposed Control Strategy

It is proposed to modify a plant conformed by an *LCL* filter with resonance frequency $\omega^L_{\rm res}$, in such a way that it behaves similarly to an *LCL* filter with a desired resonance $\omega^H_{\rm res}$ within the range $0.228\,\omega_s \le \omega^H_{\rm res} \le 0.454\,\omega_s$. Based on the explanation given in Section III, the system obtained will be able to be controlled using the PR regulator optimum design. In addition, as has been seen, with an appropriate choice of $\omega^H_{\rm res} > \omega_{\rm crit}$, it is possible to obtain a closed-loop system response very similar to that obtained when an *L* filter is controlled. Such modification of the plant can be implemented using reference model control techniques [26].

By factoring the numerator of (3), the following general expression for the discrete plant with resonance frequency $\omega^X_{\rm res}$ can be obtained

$$G^X(z) = \frac{\vec{i}_2(z)}{\vec{v}_c(z)} = \frac{P^X(z)}{Q^X(z)} = \frac{K^X(z - z^X_{\rm st})(z - 1/z^X_{\rm st})}{z(z-1)(z^2 + q^X z + 1)} \quad (7)$$

where superscript $X = L$ or $X = H$ when making reference to a filter with resonance frequency $\omega^L_{\rm res}$ or $\omega^H_{\rm res}$, respectively. $P^X(z)$ and $Q^X(z)$ are the respective polynomials numerator and denominator of $G^X(z)$. K^X and $q^X = -2z\cos(\omega^X_{\rm res}T_s) \in \mathbb{R}$. $z^X_{\rm st} = (-h^X + \sqrt{(h^X)^2 - 1})$ with $h^X = (b^X - d^X)/(1 - b^X)$, $d^X = \cos(\omega^X_{\rm res}T_s)$, and $b^X = \sin(\omega^X_{\rm res}T_s)/(\omega^X_{\rm res}T_s)$.

Note that (7) has two reciprocal zeros ($z^X_{\rm st}$ and $1/z^X_{\rm st}$). It is easy to demonstrate that, for a filter with a resonance frequency less than the Nyquist frequency ($\omega^X_{\rm res} < \omega_s/2$), it is always $0 < b^X < 1$ and $1 < h^X < 2$. Therefore, $z^X_{\rm st} \in \mathbb{R}$, $-1 < z^X_{\rm st} < (-2 + \sqrt{3}) \approx -0.27$. This means that, in the resonance frequency range of interest, the zero $z^X_{\rm st}$ will be always located within the unit circle, and therefore, the reciprocal zero $1/z^X_{\rm st}$ will be located outside the circle.

Fig. 5 illustrates the block diagram of the proposed controller in this paper for the system of Fig. 1. The transfer function of plant $G^L(z)$ [(7) with $X = L$], consists of a numerator $P^L(z)$ whose degree is 2 and a denominator $Q^L(z)$ whose degree is 4. Let $C(z) = c_2z^2 + c_1z + c_0$, $D(z) = d_3z^3 + d_2z^2 + d_1z + d_0$, and K_a a gain. Also, let $\Lambda(z) = z^3 + \lambda_2z^2 + \lambda_1z + \lambda_0$, a stable arbitrary monic polynomial. The transfer function of the block "Modified Plant" in Fig. 5 results

$$G^H_{\rm mod}(z) = \frac{\vec{i}_2(z)}{\vec{v}_{\rm PR}(z)} = \frac{P_m(z)}{Q_m(z)} = \frac{K_a\Lambda(z)P^L(z)}{[\Lambda(z) - C(z)]Q^L(z) - P^L(z)D(z)}. \quad (8)$$

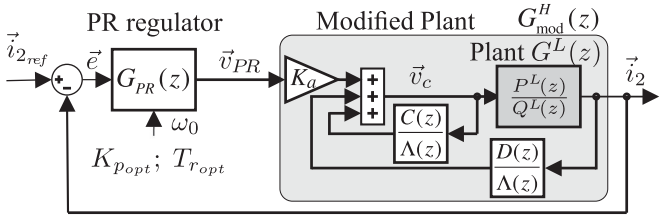

Fig. 5. Block diagram of the proposed controller.

This transfer function has a numerator polynomial $P_m(z)$ whose degree is 5, and a denominator polynomial $Q_m(z)$ whose degree is 7. Since there are 7 coefficients [three of $C(z)$ and four of $D(z)$], for a given $\Lambda(z)$, there are enough degrees of freedom to assign the seven poles in (8) [26]. The expression $Q_m(z) = [\Lambda(z) - C(z)]Q^L(z) - P^L(z)D(z)$, is a Diophantine equation [32] wherein $Q^L(z)$ and $P^L(z)$ are coprime (no common roots). The coefficients that $[\Lambda(z) - C(z)]$ and $D(z)$ must have to obtain a desired polynomial $Q_m(z)$ whose degree is 7, can be found solving the matrix equation (13) (see Appendix).

It would be desirable that the transfer function (8) results equal to the transfer function $G^H(z)$ [(7) with $X = H$]. This cannot be achieved since it is not possible to cancel the zero $1/z^L_{\rm st}$ of $G^L(z)$ (since it is outside the unit circle). However, it is possible to obtain a system with a behavior very close to that of $G^H(z)$. If $Q_m(z) = \Lambda(z)Q^H(z)$ is selected, the transfer function of the "Modified Plant" results

$$G^H_{\rm mod}(z) = K_a \frac{P^L(z)}{Q^H(z)} = \frac{K_a K^L (z - z^L_{\rm st})(z - 1/z^L_{\rm st})}{z(z-1)(z^2 + q^H z + 1)} \quad (9)$$

with $q^H = -2z\cos(\omega^H_{\rm res} T_s)$. It should be noted that the "Modified Plant" is not a stable closed-loop system, on the contrary, it is an inherently unstable system that must be stabilized using the PR regulator. The transfer function (9), retains the zeros of $G^L(z)$ and has the poles of $G^H(z)$. It can be demonstrated that two reciprocal real zeros ($z^X_{\rm st}$ and $1/z^X_{\rm st}$) always provide the same phase regardless of their location. Therefore, the phase behavior of $G^H_{\rm mod}(z)$ will be identical to that of $G^H(z)$. It is desirable to preserve the bandwidth obtained when $G^H(z)$ is controlled using the PR optimum design. In order to achieve this, the constant K_a must be calculated in such a way that $G^H_{\rm mod}(z)$ has the same gain as $G^H(z)$ at the crossover frequency $\omega_c = \omega_s/12$

$$K_a = \left.\frac{P^H(z)}{P^L(z)}\right|_{z=e^{j\omega_c T}} = \frac{K^H}{K^L} \left\| \frac{(z - z^H_{\rm st})(z - 1/z^H_{\rm st})}{(z - z^L_{\rm st})(z - 1/z^L_{\rm st})} \right\|_{z=e^{j\omega_c T}}. \quad (10)$$

With this value of K_a, $G^H_{\rm mod}(z)$, and $G^H(z)$ will differ slightly in their high frequency magnitude behavior. In order to show this, consider two plants with resonance frequencies $\omega^{L_1}_{\rm res} = 0.14\omega_s$ and $\omega^{L_2}_{\rm res} = 0.47\,\omega_s$, respectively. For both plants, the corresponding "Modified Plants" (9), $G^H_{\rm mod\,1}(z)$ and $G^H_{\rm mod\,2}(z)$ with resonance frequency $\omega^H_{\rm res} = 0.36\,\omega_s$, were obtained. Fig. 6(a) shows the open-loop magnitude frequency response of the PR optimum design. Also, in this figure "Plants"

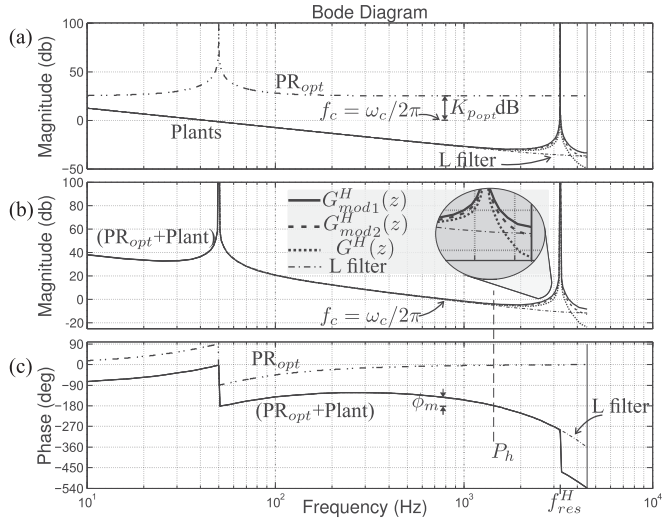

Fig. 6. Bode diagrams: (a) Magnitude for $\rm PR_{opt}$ and Plants. (b) Magnitude for cascaded systems ($\rm PR_{opt}$+Plant) (c) Phase for $\rm PR_{opt}$ and cascaded systems. For $G^{L_1}(z)$ with $\omega^{L_1}_{\rm res} = 0.14\,\omega_s$ and $G^{L_2}(z)$ with $\omega^{L_2}_{\rm res} = 0.47\,\omega_s$ modified to $G^H_{\rm mod\,1}(z)$ and $G^H_{\rm mod\,2}(z)$, respectively, with $\omega^H_{\rm res} = 0.36\,\omega_s$. Comparison with $G^H(z)$ with $\omega^H_{\rm res} = 0.36\,\omega_s$ and an *L* filter.

indicates the magnitude of the obtained "Modified Plants" along with—for comparison purposes—the magnitude of the plant $G^H(z)$ and the *L* filter. Fig. 6(b) shows the open-loop magnitude frequency responses of each plant cascaded with the optimum PR ($\rm PR_{opt}$+Plant). Fig. 6(c) shows the open-loop phase frequency responses of the PR optimum design and those corresponding to the cascaded systems.

Note that at the crossover frequency $f_c = \omega_c/2\pi$, all cascaded systems have a positive phase margin ϕ_m, practically the same as the *L* filter system. Also, note that all cascaded systems have a magnitude less than unity when the phase crosses -180° (Ph line in Fig. 6) and -540° (at the Nyquist frequency). This ensures that all cascaded systems in Fig. 6 are stable in closed-loop configuration [33].

It can also be observed in Fig. 6(b) that all magnitude plots overlap below f_c, and these exhibit only a slight difference in high frequency (close to $\omega_s/2$). Furthermore, it is observed that all phase plots are the same below f_c. These two facts imply that all plotted systems have the same bandwidth and will have the same behavior at low frequencies when in closed loop.

V. Criterion for $\omega^H_{\rm res}$ Selection

As has been seen in Section III, when a plant $G^H(z)$ with resonance frequency $\omega^H_{\rm res} = 0.36\,\omega_s$ is controlled with the PR optimum design, its closed-loop response is very similar to that of an *L* filter controlled with the PR optimum design [see Fig. 4(b) and (d)]. For this reason, it is desirable to assign this resonance frequency to the "Modified Plant" $G^H_{\rm mod}(z)$. However, this is not always possible in practice. It is well known that every inverter switch operates with a duty cycle taking values between 0 and 1. The maximum value of each duty cycle is proportional

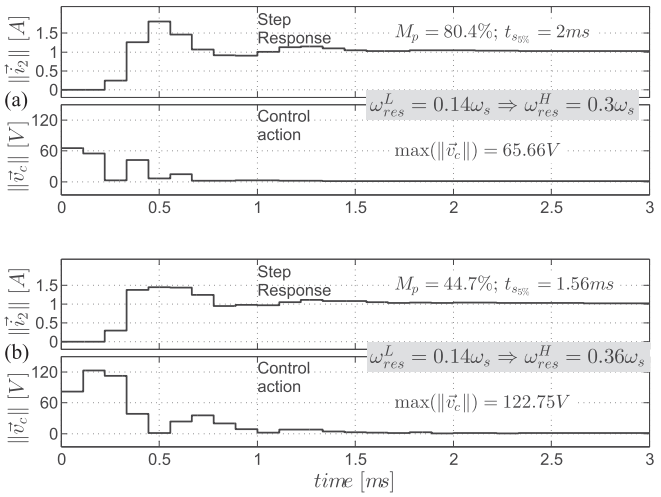

Fig. 7. Step response and control action for a system with $\omega_{\rm res}^L = 0.14\,\omega_s$ modified to: (a) $\omega_{\rm res}^H = 0.3\,\omega_s$ and (b) $\omega_{\rm res}^H = 0.36\,\omega_s$.

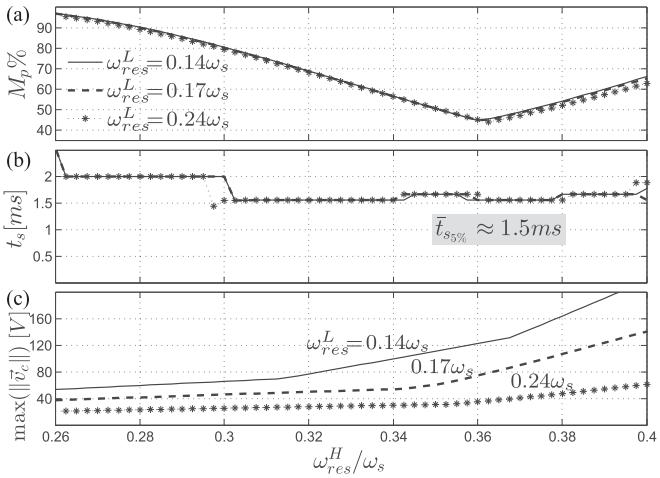

Fig. 8. Step response of the system of Fig. 5 as a function of $\omega_{\rm res}^H/\omega_s$, for $\omega_{\rm res}^L = 0.14\,\omega_s$, $0.17\,\omega_s$, and $0.24\,\omega_s$: (a) M_p, (b) $t_{s_{5\%}}$ y, (c) $\max(\|\vec{v}_c\|)$.

to the relationship between the peak value of the control action $\vec{v}_c$ and $V_{\rm bus}$. Duty cycle saturation of any switch can cause system instability. In order to prevent this, the maximum value of $\|\vec{v}_c\|$ should be limited. In this application, the larger the ratio between $\omega_{\rm res}^H$ and $\omega_{\rm res}^L$, the larger the control action $\vec{v}_c$. In order to show this, consider in Fig. 5, a plant $G^L(z)$ with $L_T = 3.78$ mH [see (3)] and resonance frequency $\omega_{\rm res}^L = 0.14\,\omega_s$. Fig. 7 shows the output current vector magnitude $\|\vec{i}_2\|$ and the control action vector magnitude $\|\vec{v}_c\|$, when a unit step is performed to the magnitude of $\vec{i}_{2_{\rm ref}}$. Fig. 7(a) corresponds to the case in which a resonance frequency $\omega_{\rm res}^H = 0.3\,\omega_s$ is selected for $G_{\rm mod}^H(z)$, and Fig. 7(b) corresponds to the case in which $\omega_{\rm res}^H = 0.36\,\omega_s$ is selected. Note that for $\omega_{\rm res}^H = 0.36\,\omega_s$ a response with less overshoot (M_p) is obtained, but the maximum control action magnitude $\max(\|\vec{v}_c\|)$ required in that case is almost twice the required when $\omega_{\rm res}^H = 0.3\,\omega_s$ is selected.

To further analyze the effect of the ratio between $\omega_{\rm res}^H$ and $\omega_{\rm res}^L$ on the dynamic response of the system and required control action, consider the three resonance frequencies of the plant $G^L(z)$: $\omega_{\rm res}^L = 0.14\,\omega_s$, $\omega_{\rm res}^L = 0.17\,\omega_s$, and $\omega_{\rm res}^L = 0.24\,\omega_s$. For these frequencies the step response of the system shown in Fig. 5 was obtained by simulation, for a set of $\omega_{\rm res}^H$ values within the following range $0.26\,\omega_s < \omega_{\rm res}^H < 0.4\,\omega_s$. In Fig. 8, it is plotted: 1) M_p, 2) $t_{s_{5\%}}$, and 3) $\max(\|\vec{v}_c\|)$ as a function of the normalized frequency $\omega_{\rm res}^H/\omega_s$. Note in Fig. 8(a) that for the three $\omega_{\rm res}^L$ considered, the minimum overshoot is obtained for a frequency $\omega_{\rm res}^H \approx 0.36\,\omega_s$, and has a value $M_{p_{\rm min}} \approx 45\%$. Note also in Fig. 8(b), that the settling time does not vary too much as a function of the $\omega_{\rm res}^H$ variation, and stays close to $\bar{t}_{s_{5\%}} \approx 1.5$ ms for $\omega_{\rm res}^H \gtrsim 0.3\,\omega_s$. On the other hand, Fig. 8(c) confirms that for each value of $\omega_{\rm res}^H$, the lower the value of $\omega_{\rm res}^L$, the larger the control action required. Therefore, given a plant $G^L(z)$ with resonance frequency $\omega_{\rm res}^L$, the choice of $\omega_{\rm res}^H$ will be a tradeoff between the step response overshoot, and the control action applied to the plant. The criterion for $\omega_{\rm res}^H$ selection can be summarized as: if it is possible, select $\omega_{\rm res}^H = 0.36\,\omega_s$. If it is not possible because of the control action limitation, then select the nearest down frequency whose implementation requires an acceptable control action.

TABLE I
RESONANCE FREQUENCIES UNDER STUDY

Case	$\omega_{\rm res}^L$	Region	$\omega_{\rm res}^H$
A	$0.14\,\omega_s$	Low frequency ($< \omega_{\rm crit}$)	$0.3\,\omega_s$
B	$0.17\,\omega_s$	Critical frequency ($\approx \omega_{\rm crit}$)	$0.345\,\omega_s$
C	$0.24\,\omega_s$	Optimal ($0.228\,\omega_s \lesssim \omega_{\rm res}^L \lesssim 0.454\,\omega_s$)	$0.36\,\omega_s$

TABLE II
PARAMETERS OF THE EXPERIMENTAL AND SIMULATION SYSTEM

Symbol	Value	Symbol	Value
$V_{\rm bus}$	400 V	t_D	0.7 μs
V_{g_ϕ}	$(100/\sqrt{2})V_{\rm rms}$	$\omega_{\rm res}^L/\omega_s$	0.14/0.17/0.24
ω_0	2π (50 Hz)	$L_1\,;L_2$	2.28 mH 1.5 mH
f_s	9 kHz	C	18 μ/12 μ/6 μF
$f_{\rm pwm}$	9 kHz	f_c	$\omega_c/2\pi = 750$ Hz
$K_{p_{\rm opt}}$	17.813 Ω	$T_{r_{\rm opt}}$	2.122 ms

VI. SIMULATION RESULTS

In this section, the implementation of the proposed control strategy for the three study cases (A, B, and C) of Table I is simulated. In order to obtain results in a realistic scenario, the whole system depicted in Fig. 1 was simulated. In Table II are the parameters used in the simulation. The inverter was simulated using Insulated Gate Bipolar Transistors (IGBTs) switching to a frequency $f_{\rm pwm}$ with turn-on dead time t_D. The three *LCL* filters were built with the same values of L_1 and L_2, and the corresponding value of resonance frequency was obtained changing the value of C. Table II also lists the values of the sampling frequency $f_s = \omega_s/2\pi$, the crossover frequency $f_c = \omega_c/2\pi$ (with

TABLE III
$C(z)$, $D(z)$, AND K_a USED IN EACH STUDY CASE

Case	$C(z)$	$D(z)$	K_a
A	$-1.9067(z^2+0.4099z+0.07373)$	$16.629z(z-1)(z+2.364)$	3.6614
B	$-2.0908(z^2+0.3696z+0.0576)$	$38.402z(z-1)(z+0.5959)$	3.0023
C	$-1.4003(z+0.249)(z-0.1784)$	$32.897z(z-1)(z-0.1902)$	1.7367

$\omega_c = \omega_s/12$), and the PR optimum design parameters $K_{p_{\rm opt}}$ and $T_{r_{\rm opt}}$ obtained using (6).

Each one of the three filters of Table I was modified following the procedure described in Section IV, to behave as a system $G^H_{\rm mod}(z)$ with a specific resonance frequency $\omega^H_{\rm res}$ (column 4 of Table I). For each case, a stable monic polynomial $\Lambda(z) = z(z-z_1)(z-z_2)$ with $z_{1,2} = e^{(-0.6\pm\sqrt{0.6^2-1})\,\omega^L_{\rm res}T_s}$ was used for the controller of Fig. 5. The used polynomials $C(z)$ and $D(z)$ (calculated according to Appendix), and the used values for the constant K_a [(10)] are listed in Table III.

For each case, the injection of three-phase sinusoidal balanced current to a grid with a voltage $\vec{v}_{g_{abc}}$, was simulated. This grid voltage is shown in Fig. 9(a). In order to test the performance of the controller under grid disturbance conditions, the steady-state grid waveform was contaminated with a total harmonic distortion THD $= 3.65\%$. Also, a short time abrupt amplitude reduction of 10% (sag fail) and the manifestation of a high-harmonic distortion (HHD) close to the resonance frequency of the filter were applied [gray regions in Fig. 9(a)].

Current $\vec{i}_{2_{\rm ref}}$ was increased from 8 to 10 A (peak), in $t = 0.11$ s. For that instant, Fig. 9(b) shows the response of current $\vec{i}_{2_{abc}}$ and its magnitude $\|\vec{i}_{2_{abc}}\| = \sqrt{i_a^2+i_b^2+i_c^2}$, for the filter with $\omega^L_{\rm res} = 0.14\,\omega_s$ (case A), and Fig. 9(c) shows $\vec{i}_{2_{abc}}$ and $\|\vec{i}_{2_{abc}}\|$ for the filter with $\omega^L_{\rm res} = 0.17\,\omega_s$ (case B). For these two cases, in order to limit the control action [see Fig. 8(c)], the resonance frequencies of the "Modified Plant" were set to $\omega^H_{\rm res} = 0.3\,\omega_s$ and $\omega^H_{\rm res} = 0.345\,\omega_s$, respectively. Fig. 9(b) and (c) show that the proposed control strategy allows to control *LCL* filters with $\omega^L_{\rm res} \le \omega_{\rm crit}$.

The proposed strategy is also useful for controlling *LCL* filters that do not possess a low resonance frequency (with $\omega^L_{\rm res} > \omega_{\rm crit}$) since it allows to obtain a better dynamic response compared with that obtained when the same filter is controlled using only a PR regulator. Indeed, in Fig. 4(a) it was shown that a system with $\omega^L_{\rm res} = 0.24\omega_s > \omega_{\rm crit}$ (frequency analyzed in Case C) is stable when it is controlled with the PR optimum design. However, a poor dynamic response of the closed-loop system is obtained. For this resonance frequency, Fig. 9(d) shows the response of $\vec{i}_{2_{abc}}$ and $\|\vec{i}_{2_{abc}}\|$ when the filter is controlled using the proposed strategy (Case C). In this case, for the "Modified Plant" $G^H_{\rm mod}(z)$, the resonance frequency was set to $\omega^H_{\rm res} = 0.36\,\omega_s$, which minimizes the overshoot [see Fig. 8(a)]. Comparing the values of M_p and $t_{s_{5\%}}$ in Fig. 9(d) with those in Fig. 4(a), it is verified that the proposed control strategy significantly improves the dynamic system response in a system with these characteristics.

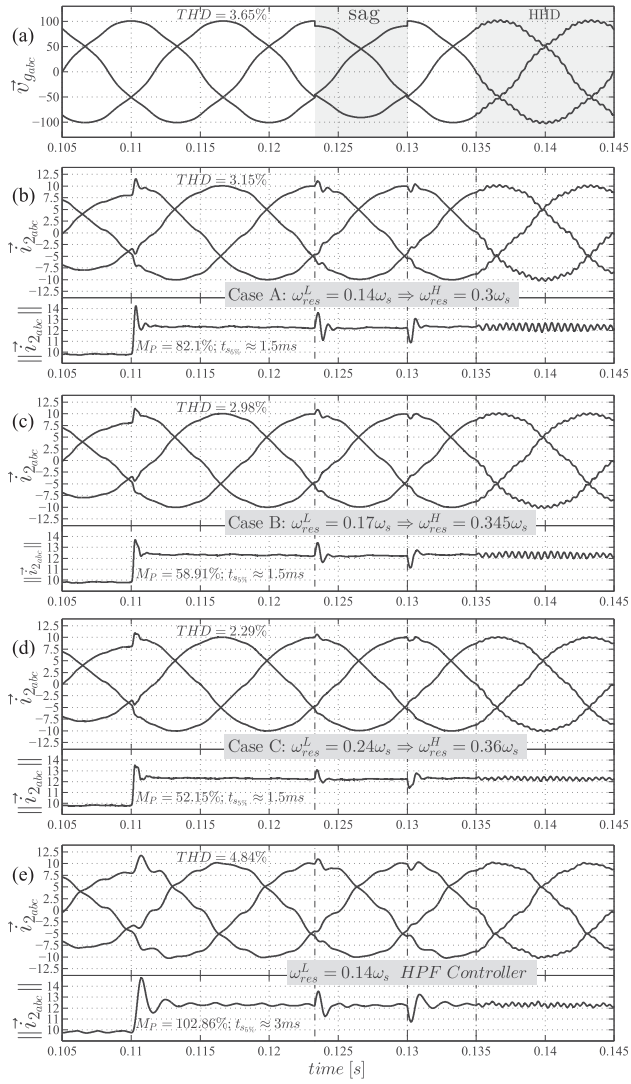

Fig. 9. Simulation results. (a) $\vec{v}_{g_{abc}}$ [V]. (b) $\vec{i}_{2_{abc}}$ [A] and $\|\vec{i}_{2_{abc}}\|$ [A] for case A. (c) $\vec{i}_{2_{abc}}$ [A] and $\|\vec{i}_{2_{abc}}\|$ [A] for case B. (d) $\vec{i}_{2_{abc}}$ [A] and $\|\vec{i}_{2_{abc}}\|$ [A] for case C. (e) $\vec{i}_{2_{abc}}$ [A] and $\|\vec{i}_{2_{abc}}\|$ [A], filter with $\omega^L_{\rm res} = 0.14\,\omega_s$ whenthe design proposed in [14] is used for the controller of Fig. 2(b).

In [14], the controller shown in Fig. 2(b) was designed for controlling an *LCL* filter with $\omega^L_{\rm res} = 0.14\,\omega_s$. The values $K_p = 0.48\ K_{p_{\rm opt}}$ and $T_r = 0.87\ T_{r_{\rm opt}}$ were used for the PR regulator constant parameters in (5); and $k_{ad} = 0.8\ K_{p_{\rm opt}}$ and $\omega_{ad} = 0.15\,\omega_s$ were used for the parameters of the HPF filter (of continuous transfer function $G_{\rm HPF}(s) = -k_{ad}s/(s+\omega_{ad})$ [14]). Fig. 9(e) shows $i_{2_{abc}}$ and $\|i_{2_{abc}}\|$, when the controller designed in [14] is used. Comparing Fig. 9(b) and (e), it can be seen that the controller proposed in this paper allows to obtain a dynamic response with less overshoot and settling time than that obtained with the controller proposed in [14]. In addition, the controller presented here shows a better rejection of the low frequency harmonics (commonly presented in the grid). Note that all systems can support both a voltage sag and an HHD grid perturbation.

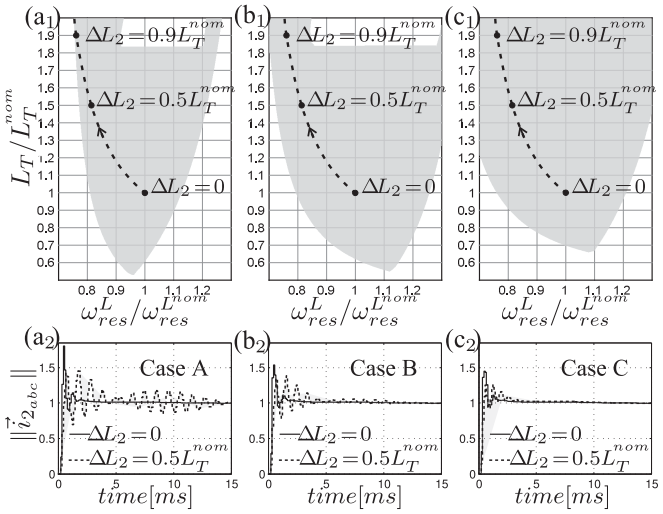

Fig. 10. Robustness analysis. Stability regions: (a_1) Case A; (b_1) B; (c_1) C. Step responses for $\Delta L_2 = 0$ and $\Delta L_2 = 0.5 L_T^{\text{nom}}$: ($a_2$) Case A; ($b_2$) B; ($c_2$) C.

A. Robustness Analysis

For study cases A, B, and C (see Table I) simulated previously, the coefficients of the proposed controller were obtained considering the nominal values of parameters $L_1 = L_1^{\text{nom}}$, $L_2 = L_2^{\text{nom}}$, and $C = C^{\text{nom}}$ listed in Table II. When the real values of the parameters differ with respect to the nominal values of design, the simulated systems may became unstable. In order to perform an analysis of the system robustness, these parameters are considered within the following bounded sets: $L_{1_{\min}} \leq L_1 \leq L_{1_{\max}}$, $L_{2_{\min}} \leq L_2 \leq L_{2_{\max}}$, and $C_{\min} \leq C \leq C_{\max}$. For each combination of parameters $\{L_1, L_2, C\}$, the closed-loop system of Fig. 5 will be stable if all its poles are located inside the unit circle. Note that the *LCL* filter transfer function (3) can be characterized (for a given value of T_s) using parameters ω_{res}^L and L_T. The bounded sets of variation of parameters $\{L_1, L_2, C\}$ can be mapped into a corresponding bounded set of variation of parameters $\{\omega_{\text{res}}^L, L_T\}$. This set is given by

$$L_{1_{\min}} + L_{2_{\min}} \leq L_T \leq L_{1_{\max}} + L_{2_{\max}}$$

$$\sqrt{\frac{L_{1_{\max}} + L_{2_{\max}}}{L_{1_{\max}} L_{2_{\max}} C_{\max}}} \leq \omega_{\text{res}}^L \leq \sqrt{\frac{L_{1_{\min}} + L_{2_{m\,\min}}}{L_{1_{\min}} L_{2_{\min}} C_{\min}}}.$$

Let $\omega_{\text{res}}^{L^{\text{nom}}}$ and L_T^{nom} be the nominal values of ω_{res}^L and L_T, respectively; the shaded regions shown in Fig. 10 (a_1)–(c_1) correspond to the normalized regions $\{\omega_{\text{res}}^L / \omega_{\text{res}}^{L^{\text{nom}}}, L_T / L_T^{\text{nom}}\}$ where the closed-loop system of Fig. 5 is stable for each one of the three study cases. It can be observed that all cases support different ranges of variation in both ω_{res}^L and L_T. Usually the grid connection increases the effective inductance L_2 of the *LCL* filter [11], [34]. In order to analyze the robustness in presence of a grid inductance variation, the dotted lines in Fig. 10(a_1)–(c_1) correspond to the points $\{\omega_{\text{res}}^L / \omega_{\text{res}}^{L^{\text{nom}}}, L_T / L_T^{\text{nom}}\}$ such that L_2 is increased while the other parameters are kept at their nominal values. Note that in Case A the system remains in the

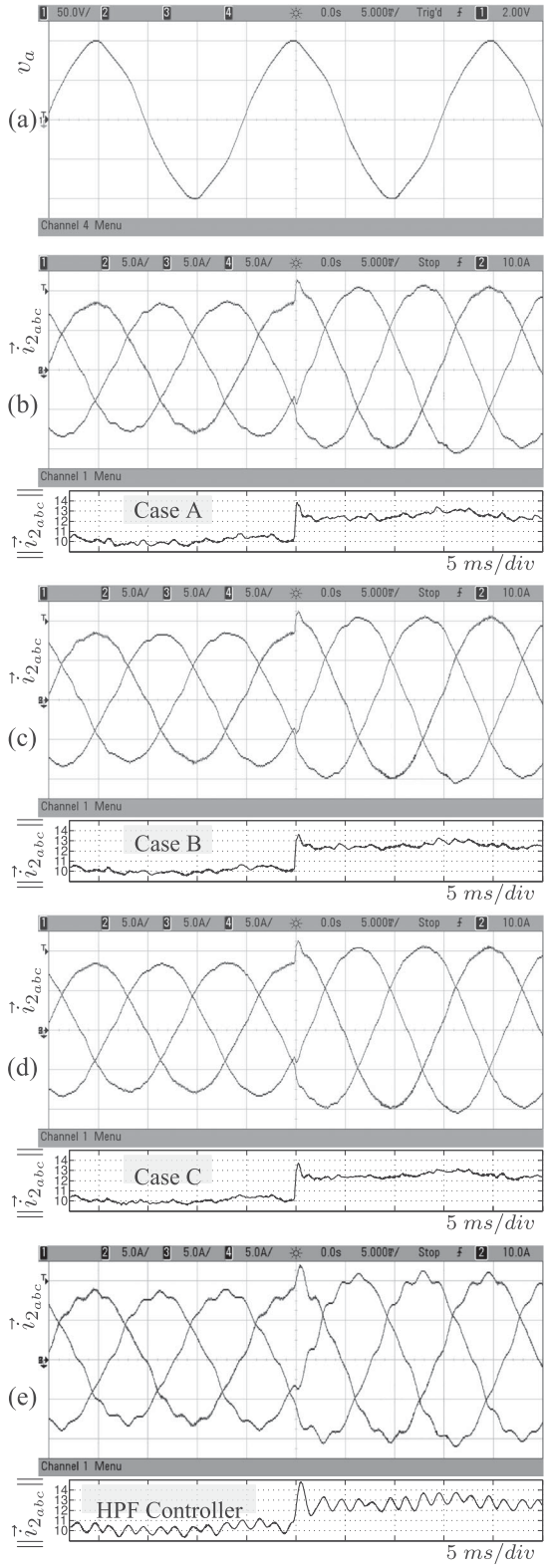

Fig. 11. Experimental results. (a) $\vec{v}_{g_{abc}}$ [V] (phase "a"). (b) $\vec{i}_{2_{abc}}$ [A] and $\|\vec{i}_{2_{abc}}\|$ [A] for Case A. (c) $\vec{i}_{2_{abc}}$ [A] and $\|\vec{i}_{2_{abc}}\|$ [A] for Case B. (d) $\vec{i}_{2_{abc}}$ [A] and $\|\vec{i}_{2_{abc}}\|$ [A] for Case C. (e) $\vec{i}_{2_{abc}}$ [A] and $\|\vec{i}_{2_{abc}}\|$ [A], filter with $\omega_{\text{res}}^L = 0.14\,\omega_s$ when the design proposed in [14] is used for the controller of Fig. 2(b). Oscilloscope screenshots voltage scale: 50 V/div, current scale: 5 A/div, time scale: 5 ms/div.

stable region for a deviation up to $\Delta L_2 = 0.9 L_T^{\text{nom}}$, while the other systems support even greater deviations. In order to test the robustness Fig. 10(a_2)–(c_2) show for each study case, the step responses of the closed-loop systems for $\Delta L_2 = 0$ and $\Delta L_2 = 0.5\, L_T^{\text{nom}}$. Clearly the Case A is the most sensitive to parametric variations, however, this system remains stable despite a large grid inductance deviation.

VII. Experimental Results

This section presents the experimental results obtained from the practical implementation of the three study cases (A, B, and C) simulated in Section VI. These results were obtained using a three-phase inverter prototype built using IGBT devices IRG4PH50UD. The controller was implemented in a fixed-point digital signal processor TMS320F2812. The parameters of the experimental system are listed in Table II and are the same that were used previously to obtain the simulation results. In the three study cases, a three-phase sinusoidal balanced current was injected to a grid with voltage $\vec{v}_{g_{abc}}$. Fig. 11(a) shows phase "a" of $\vec{v}_{g_{abc}}$.

For comparison purposes, the tests simulated in Section VI were experimentally repeated. Fig. 11(b) shows the response of current $\vec{i}_{2_{abc}}$ and its magnitude $\|\vec{i}_{2_{abc}}\|$ (obtained using the stored screenshot data values) for Case A; Fig. 11(c) shows $\vec{i}_{2_{abc}}$ and $\|\vec{i}_{2_{abc}}\|$ for Case B; and Fig. 11(d) shows $\vec{i}_{2_{abc}}$ and $\|\vec{i}_{2_{abc}}\|$ for Case C. Fig. 11(e) shows $i_{2_{abc}}$ and $\|\vec{i}_{2_{abc}}\|$, when the controller designed in [14] is used. Note that the experimental results shown in Fig. 11 are similar to those shown in Fig. 9 obtained by simulation. Therefore, the conclusions drawn for the simulation results are also valid for the experimental results. Particularly, the comparison between Fig. 9(d) and (e) corroborates experimentally that the controller presented in this paper achieves better response than the one used in [14].

VIII. Conclusion

This paper presents a control strategy that allows to regulate the current injected into the grid by a three-phase inverter with a low resonance frequency *LCL* filter, without passive damping. The strategy uses a PR regulator optimum design and only requires the measurement of the current injected to the grid. Both simulation and experimental results were presented. The performance of the controller was evaluated, comparing it with a control method recently proposed in the literature for controlling the same system. The proposal presented here offers better closed-loop dynamic response and better disturbance rejection.

Appendix

Let $A(z) = a_n z^n + a_{n-1} z^{n-1} + \cdots + a_0$ and $Q(z) = q_m z^m + q_{m-1} z^{m-1} + \cdots + q_0$ be two polynomials in z, whose degrees are n and m, respectively, with $m \geq n \geq 1$. Let $B(z) = b_k z^k + b_{k-1} z^{k-1} + \cdots + b_0$ be a polynomial whose degree is $k \leq (m - n + 1)$.

Proposition: If $A(z)$ and $B(z)$ are coprime, then there exist unique polynomials $L(z) = l_{m-n} z^{m-n} + \cdots + l_0$ and $P(z) = p_{n-1} z^{n-1} + \cdots + p_0$ whose degrees are $(m - n)$ and $(n - 1)$, respectively, that verify the Diophantine equation

$$A(z)L(z) + B(z)P(z) = Q(z). \tag{11}$$

Proof: Equating coefficients on both sides of (11), it results

$$\overbrace{\left[\begin{array}{cccc|cccc} a_n & 0 & \cdots & 0 & 0 & 0 & 0 & 0 \\ a_{n-1} & a_n & \cdots & 0 & \vdots & \vdots & \ddots & \vdots \\ \vdots & a_{n-1} & \cdots & 0 & b_k & 0 & \cdots & 0 \\ a_0 & \vdots & \cdots & \vdots & b_{k-1} & b_k & \cdots & 0 \\ 0 & a_0 & \cdots & 0 & \vdots & b_{k-1} & \cdots & 0 \\ 0 & 0 & \cdots & a_n & b_0 & \vdots & \cdots & b_k \\ \vdots & \vdots & \ddots & a_{n-1} & 0 & b_0 & \cdots & b_{k-1} \\ 0 & 0 & \cdots & \vdots & \vdots & \vdots & \ddots & \vdots \\ 0 & 0 & \cdots & a_0 & 0 & 0 & \cdots & b_0 \end{array}\right]}^{\mathbf{M}} \overbrace{\begin{bmatrix} l_{m-n} \\ l_{m-n-1} \\ l_{m-n-2} \\ \vdots \\ l_0 \\ p_{n-1} \\ p_{n-2} \\ \vdots \\ p_0 \end{bmatrix}}^{\mathbf{\Theta}} = \overbrace{\begin{bmatrix} q_m^* \\ q_{m-1}^* \\ q_{m-2}^* \\ \vdots \\ \vdots \\ \vdots \\ \vdots \\ q_1 \\ q_0 \end{bmatrix}}^{\mathbf{\Theta}^*}$$

$$\underbrace{\qquad\qquad}_{(m-n+1)\text{ col.}} \qquad \underbrace{\qquad\qquad}_{n\text{ col.}} \tag{12}$$

where $\mathbf{M} \in \Re^{(m+1)\times(m+1)}$, $\mathbf{\Theta} \in \Re^{(m+1)\times 1}$, and $\mathbf{\Theta}^* \in \Re^{(m+1)\times 1}$. If $A(z)$ and $B(z)$ are coprime, it must be $det(\mathbf{M}) \neq 0$. This can be demonstrated by a similar procedure to that carried out in [32]. Therefore, matrix $\mathbf{M}$ is invertible, and from (12), given a $Q(z)$ whose degree is m, the unique coefficients of $L(z)$ and $P(z)$ that satisfy the Diophantine equation (11) can be determined solving the following matrix equation :

$$\mathbf{\Theta} = \mathbf{M}^{-1} \mathbf{\Theta}^*. \tag{13}$$

References

[1] *IEEE Recommended Practices and Requirements for Harmonic Control in Electrical Power Systems*, *IEEE Standard 519-1992*, Apr. 1993.

[2] A. Prudenzi, U. Grasselli, and R. Lamedica, "IEC Std. 61000-3-2 harmonic current emission limits in practical systems: Need of considering loading level and attenuation effects," in *Proc. Power Eng. Soc. Summer Meeting*, 2001, vol. 1, pp. 277–282.

[3] *IEEE Standard for Interconnecting Distributed Resources With Electric Power Systems*," *IEEE Standard 1547-2003*, Jul. 2003.

[4] R. Peña Alzola, M. Liserre, F. Blaabjerg, R. Sebastián, J. Dannehl, and F. Fuchs, "Analysis of the passive damping losses in LCL-filter-based grid converters," *IEEE Trans. Power Electron.*, vol. 28, no. 6, pp. 2642–2646, Jun. 2013.

[5] R. N. Beres, X. Wang, M. Liserre, F. Blaabjerg, and C. L. Bak, "A review of passive power filters for three-phase grid-connected voltage-source converters," *IEEE J. Emerg. Sel. Topics Power Electron.*, vol. 4, no. 1, pp. 54–69, Mar. 2016.

[6] J. Dannehl, F. Fuchs, S. Hansen, and P. Thøgersen, "Investigation of active damping approaches for PI-based current control of grid-connected pulse width modulation converters with LCL filters," *IEEE Trans. Ind. Appl.*, vol. 46, no. 4, pp. 1509–1517, Jul. 2010.

[7] Y. Tang, P. C. Loh, P. Wang, F. H. Choo, and F. Gao, "Exploring inherent damping characteristic of LCL-filters for three-phase grid-connected voltage source inverters," *IEEE Trans. Power Electron.*, vol. 27, no. 3, pp. 1433–1443, Mar. 2012.

[8] C. Bao, X. Ruan, X. Wang, W. Li, D. Pan, and K. Weng, "Step-by-step controller design for LCL-type grid-connected inverter with capacitor-current-feedback active-damping," *IEEE Trans. Power Electron.*, vol. 29, no. 3, pp. 1239–1253, Mar. 2014.

[9] J. Dannehl, C. Wessels, and F. Fuchs, "Limitations of voltage-oriented PI current control of grid-connected PWM rectifiers with LCL filters," *IEEE Trans. Ind. Electron.*, vol. 56, no. 2, pp. 380–388, Feb. 2009.

[10] S. Parker, B. McGrath, and D. Holmes, "Regions of active damping control for LCL filters," *IEEE Trans. Ind. Appl.*, vol. 50, no. 1, pp. 424–432, Jan. 2014.
[11] X. Wang, F. Blaabjerg, and P. C. Loh, "Virtual RC damping of LCL-filtered voltage source converters with extended selective harmonic compensation," *IEEE Trans. Power Electron.*, vol. 30, no. 9, pp. 4726–4737, Sep. 2015.
[12] J. Xu, S. Xie, and T. Tang, "Active damping-based control for grid-connected LCL -filtered inverter with injected grid current feedback only," *IEEE Trans. Ind. Electron.*, vol. 61, no. 9, pp. 4746–4758, Sep. 2014.
[13] M. Hanif, V. Khadkikar, W. Xiao, and J. L. Kirtley, "Two degrees of freedom active damping technique for LCL filter-based grid connected PV systems," *IEEE Trans. Ind. Electron.*, vol. 61, no. 6, pp. 2795–2803, Jun. 2014.
[14] X. Wang, F. Blaabjerg, and P. C. Loh, "Grid-current-feedback active damping for LCL resonance in grid-connected voltage-source converters," *IEEE Trans. Power Electron.*, vol. 31, no. 1, pp. 213–223, Jan. 2016.
[15] X. Li, X. Wu, Y. Geng, X. Yuan, C. Xia, and X. Zhang, "Wide damping region for LCL-type grid-connected inverter with an improved capacitor-current-feedback method," *IEEE Trans. Power Electron.*, vol. 30, no. 9, pp. 5247–5259, Sep. 2015.
[16] Z. Xin, P. C. Loh, X. Wang, F. Blaabjerg, and Y. Tang, "Highly accurate derivatives for LCL-filtered grid converter with capacitor voltage active damping," *IEEE Trans. Power Electron.*, vol. 31, no. 5, pp. 3612–3625, May 2016.
[17] P. C. Loh and D. Holmes, "Analysis of multiloop control strategies for LC/CL/LCL-filtered voltage-source and current-source inverters," *IEEE Trans. Ind. Appl.*, vol. 41, no. 2, pp. 644–654, Mar. 2005.
[18] J. Dannehl, F. W. Fuchs, and P. B. Thøgersen, "PI state space current control of grid-connected PWM converters with LCL filters," *IEEE Trans. Power Electron.*, vol. 25, no. 9, pp. 2320–2330, Sep. 2010.
[19] C. A. Busada, S. G. Jorge, and J. A. Solsona, "Full-state feedback equivalent controller for active damping in LCL-filtered grid-connected inverters using a reduced number of sensors," *IEEE Trans. Ind. Electron.*, vol. 62, no. 10, pp. 5993–6002, Oct. 2015.
[20] J. Massing, M. Stefanello, H. Grundling, and H. Pinheiro, "Adaptive current control for grid-connected converters with LCL filter," *IEEE Trans. Ind. Electron.*, vol. 59, no. 12, pp. 4681–4693, Dec. 2012.
[21] X. Fu, S. Li, and I. Jaithwa, "Implement optimal vector control for LCL-filter-based grid-connected converters by using recurrent neural networks," *IEEE Trans. Ind. Electron.*, vol. 62, no. 7, pp. 4443–4454, Jul. 2015.
[22] D. N. Zmood and D. G. Holmes, "Stationary frame current regulation of PWM inverters with zero steady-state error," *IEEE Trans. Power Electron.*, vol. 18, no. 3, pp. 814–822, May 2003.
[23] D. Holmes, T. Lipo, B. McGrath, and W. Kong, "Optimized design of stationary frame three phase ac current regulators," *IEEE Trans. Power Electron.*, vol. 24, no. 11, pp. 2417–2426, Nov. 2009.
[24] G. Shen, X. Zhu, J. Zhang, and D. Xu, "A new feedback method for PR current control of LCL-filter-based grid-connected inverter," *IEEE Trans. Ind. Electron.*, vol. 57, no. 6, pp. 2033–2041, Jun. 2010.
[25] B. Li, W. Yao, L. Hang, and L. M. Tolbert, "Robust proportional resonant regulator for grid-connected voltage source inverter (VSI) using direct pole placement design method," *IET Power Electron.*, vol. 5, no. 8, pp. 1367–1373, Sep. 2012.
[26] G. Goodwin and K. Sang Sin, *Adaptive Filtering Prediction and Control*. New York, NY, USA: Dover, 2009.
[27] N. Hoffmann, F. Fuchs, and J. Dannehl, "Models and effects of different updating and sampling concepts to the control of grid-connected PWM converters—A study based on discrete time domain analysis," in *Proc. 14th Eur. Conf. Power Electron. Appl.*, Aug. 2011, pp. 1–10.
[28] S. Buso and P. Mattavelli, *Digital Control in Power Electronics*. San Rafael, CA, USA: Morgan & Claypool Publishers, 2006.
[29] G. Goodwin, S. Graebe, and M. E. Salgado, *Control System Design*. Englewood Cliffs, NJ, USA: Prentice Hall, 2001.
[30] J. Xu, S. Xie, and T. Tang, "Evaluations of current control in weak grid case for grid-connected LCL-filtered inverter," *IET Power Electron.*, vol. 6, no. 2, pp. 227–234, Feb. 2013.
[31] B. A. Francis and W. M. Wonham, "The internal model principle of control theory," *Automatica*, vol. 12, no. 5, pp. 457–465, Sep. 1976.
[32] P. Antsaklis and A. Michel, *Linear Systems*. New York, NY, USA: McGraw-Hill, 1997.
[33] J. Dannehl, M. Liserre, and F. W. Fuchs, "Filter-based active damping of voltage source converters with LCL filter," *IEEE Trans. Ind. Electron.*, vol. 58, no. 8, pp. 3623–3633, Aug. 2011.
[34] M. Liserre, R. Teodorescu, and F. Blaabjerg, "Stability of photovoltaic and wind turbine grid-connected inverters for a large set of grid impedance values," *IEEE Trans. Power Electron.*, vol. 21, no. 1, pp. 263–272, Jan. 2006.

Roberto A. Fantino received the Electronics Engineer and M.S. degrees from the Universidad Nacional del Sur, Bahía Blanca, Argentina, in 2011 and 2015, respectively, where he is currently working toward the Dr. degree in systems control.

He is currently in the Departamento de Ingeniería Eléctrica y de Computadoras, Instituto de Investigaciones en Ingeniería Eléctrica "Alfredo C. Desages", Universidad Nacional del Sur, Bahía Blanca, Argentina, where he is a graduate Teaching Assistant. His research and work interests include the field of power electronics, grid power control, renewable and alternative energy resources, and distributed power generation.

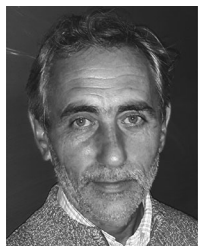

Claudio A. Busada was born in Bahía Blanca, Argentina, on March 13, 1962. He received the degree in electrical engineering, in 1989, and the Dr. degree in control systems, in 2004, both from the Universidad Nacional del Sur, Bahía Blanca, Argentina.

From 1988 to 2004, he was in the Mechanic and Electrical Department, Bahía Blanca. Since 1989, he has been in the Departamento de Ingeniería Eléctrica y de Computadoras, Universidad Nacional del Sur, where currently he is a Professor. He is a Researcher in the the Instituto de Investigaciones en Ingeniería Eléctrica "Alfredo C. Desages", Bahia Blanca, Argentina. His research interests include power electronics, rotating machinery, active filters, automatic control, and integration of distributed energy systems.

Jorge A. Solsona (SM'04) received the Electronics Engineer and Dr. in Engineering degrees from the Universidad Nacional de La Plata, La Plata, Argentina, in 1986 and 1995, respectively.

He is currently in the Departamento de Ingeniería Eléctrica y de Computadoras, Instituto de Investigaciones en Ingeniería Eléctrica "Alfredo C. Desages", Universidad Nacional del Sur, Bahía Blanca, Argentina, where he is a Professor, and with CONICET. He is involved in teaching and research on control theory and its applications to electromechanical systems.